CENTRAL RESEARCH LIBRARY

ORNL-5063

LOCKHEED MARTIN ENERGY RESEARCH LIBRARIES

3 4456 0515252 6

cy 1

An Electromagnetic Ultrasonic Transducer

Katsuhiro Kawashima

OAK RIDGE NATIONAL LABORATORY
CENTRAL RESEARCH LIBRARY
DOCUMENT COLLECTION
LIBRARY LOAN COPY
DO NOT TRANSFER TO ANOTHER PERSON
If you wish someone else to see this document, send in name with document and the library will arrange a loan.
UCN-7969
13 3-67

OAK RIDGE NATIONAL LABORATORY
OPERATED BY UNION CARBIDE CORPORATION • FOR THE U.S. ATOMIC ENERGY COMMISSION

Printed in the United States of America. Available from
National Technical Information Service
U.S. Department of Commerce
5285 Port Royal Road, Springfield, Virginia 22161
Price: Printed Copy $4.00; Microfiche $2.25

This report was prepared as an account of work sponsored by the United States Government. Neither the United States nor the Energy Research and Development Administration, nor any of their employees, nor any of their contractors, subcontractors, or their employees, makes any warranty, express or implied, or assumes any legal liability or responsibility for the accuracy, completeness or usefulness of any information, apparatus, product or process disclosed, or represents that its use would not infringe privately owned rights.

ORNL-5063
UC-25 — Materials

Contract No. W-7405-eng-26

METALS AND CERAMICS DIVISION

AN ELECTROMAGNETIC ULTRASONIC TRANSDUCER

Katsuhiro Kawashima

AUGUST 1975

OAK RIDGE NATIONAL LABORATORY
Oak Ridge, Tennessee 37830
operated by
UNION CARBIDE CORPORATION
for the
U.S. ENERGY RESEARCH AND DEVELOPMENT ADMINISTRATION

LOCKHEED MARTIN ENERGY RESEARCH LIBRARIES
3 4456 0515252 6

CONTENTS

ABSTRACT 1
INTRODUCTION 2
THE PRINCIPLE OF A TRANSDUCER 3
Experimental Method 5
Method of Operation 6
Samples 6
Driver Coil Current 7
EXPERIMENTAL RESULTS 7
Determination of the Basic Characteristics of the Transducer . 7
Flaw Detection 12
Effect of Transducer-to-Specimen Spacing 16
Effect of Horizontal Displacement 16
Wave Velocity Measurement 19
CONSIDERATIONS OF THE MODE CONVERSION 22
SUMMARY AND CONCLUSION 25
ACKNOWLEDGMENTS 25
APPENDIX . Calculation of the Ultrasonic Wave Fields Produced by the Electromagnetic Transducer 29

AN ELECTROMAGNETIC ULTRASONIC TRANSDUCER

Katsuhiro Kawashima[1]

ABSTRACT

An electromagnetic ultrasonic transducer that generates and detects a relatively large amount of longitudinal ultrasonic wave and a small amount of radially polarized transverse ultrasonic wave was built and tested on stainless steel, mild steel, and aluminum. Flaw detection ability of the electromagnetic transducer was compared with that of a piezoelectric ceramic transducer, and the signal-to-noise ratios were comparable. Finally, ultrasonic fields produced by the electromagnetic transducer were calculated including considerations about the mode conversion between a longitudinal wave and a radially polarized transverse wave.

[1]Guest from Nippon Steel Corporation, 2-6-3 Otemachi, Chiyodaku, Tokyo, Japan.

INTRODUCTION

The method of electromagnetic generation and detection of ultrasonic waves has recently been developed as a new method for applying ultrasound.[2-10] The ultrasonic wave is generated directly inside the metal by the interaction of a magnetic field and eddy currents that are induced by an induction coil placed on the metal surface. Then an interaction of the ultrasonic wave with the magnetic field gives rise to eddy currents, which are detected by an induction coil. The technique is similar to eddy-current nondestructive testing, and the physical phenomenon for detecting flaws and measuring material properties is that of ultrasonic nondestructive testing. The main advantages of this technique are summarized as follows.

1. An ultrasonic wave can be generated without any contact between a transducer and a material being tested. This characteristic is useful for materials that are at high temperatures, are moving, have rough surfaces, or must be protected from contamination by water or oil used in conventional ultrasonic testing.

2. The technique can generate ultrasonic waves of several different modes. Various combinations of the directions of the magnetic field and eddy currents can generate different ultrasonic wave modes, some of which can never be generated by a conventional ultrasonic transducer.

---

[2]E. R. Dobbs and J. D. Llewellyn, "Generation of Ultrasonic Waves Without Using a Transducer," *Non-Destr. Test. (Guilford, Engl.)* 4(1): 49–56 (February 1971).

[3]K. O. Legg and D. J. Meredith, "Flaw Detection in Metals Using Electromagnetic Sound Generation," *J. Phys. D* 3: L61–L63 (1970).

[4]E. R. Dobbs, "Electromagnetic Generation of Ultrasonic Waves in Metals," *J. Phys. Chem. Solids* 31: 1657–67 (1970).

[5]D. J. Meredith, R. J. Watts-Tobin, and E. R. Dobbs, "Electromagnetic Generation of Ultrasonic Waves in Metals," *J. Acoust. Soc. Amer.* 45(6): 1393–1401 (1969).

[6]A. G. Betjemann et al., "R. F. — Ultrasonic Wave Generation in Metals," *Phys. Lett. A* 25(10): 753–54 (1967).

[7]J. R. Houck et al., "Direct Electromagnetic Generation of Acoustic Waves," *Phys. Rev. Lett.* 19(5): 224–27 (1967).

[8]P. R. Larsen and K. Saermark, "Electromagnetic Excitation of Elastic Modes in Aluminum," *Phys. Lett. A* 26(7): 296–97 (1968).

[9]H. Wüstenberg, "Contactless Electrodynamic Ultrasonic Transducers and Their Application to Ultrasonic Inspection," pp. 37–48 in *Preprints 6. ICNT Vol. B, 1970,* Deutsche Gesellschaft für Zerstörungsfreie Prüfverfahren e.V., Berlin.

[10]R. Botsco, "The Eddy-Sonic Test Method," *Mater. Eval.* 26(2): 21–26 (February 1968).

An electromagnetic transducer that has a simple structure and can generate and detect a relatively large amount of radially polarized transverse wave simultaneously with a small amount of longitudinal wave has been made by the author.[11]

This report describes the construction of an electromagnetic transducer that generates and detects a large amount of longitudinal wave and a small amount of radially polarized transverse wave and tests of it with mild steel, stainless steel, and aluminum. The electromagnetic forces and elastic waves produced by the forces are calculated and compared with the experimental results.

THE PRINCIPLE OF A TRANSDUCER

Eddy currents induced in a material by a circular driver coil placed on its surface have only an azimuthal component, I_ϕ. The stationary magnetic flux produced by ferromagnetic steel pole pieces has a radial component, B_r, and a vertical component, B_z. (See Fig. 1.)

---

[11]Katsuhiro Kawashima, *An Electromagnetic Transducer for Generation and Detection of Both Longitudinal and Transverse Ultrasonic Waves*, ORNL-5064 (in preparation).

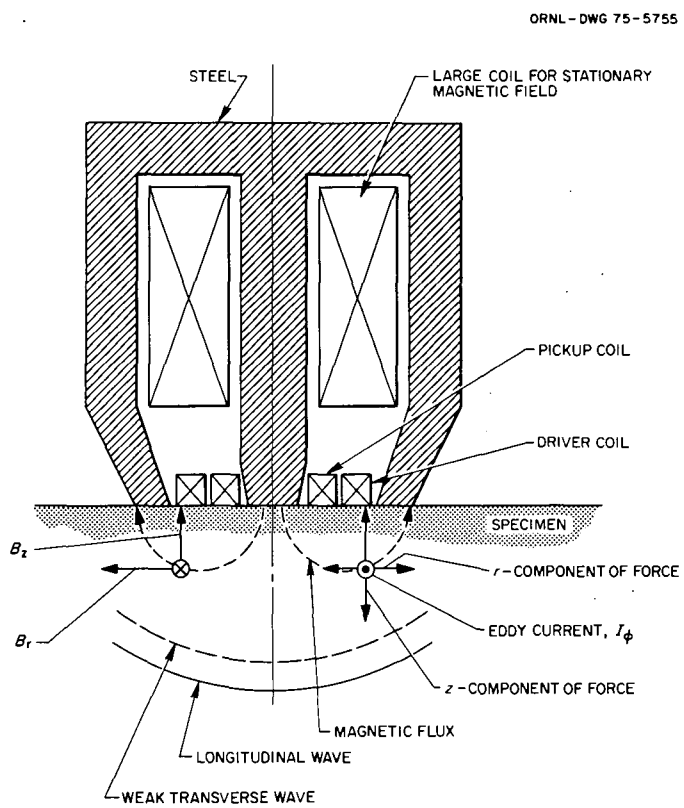

Fig. 1. The Principle of an Electromagnetic Transducer.

In the case of nonmagnetic metals, the force produced by an electromagnetic field below optical frequencies is given, to a very good approximation, by the Lorentz formula

$$\vec{F} = \vec{I} \times \vec{B} \; ;$$

the vertical component of the force is given by

$$F_z = I_\phi B_r \; ,$$

and the radial component by

$$F_r = I_\phi B_z \; .$$

If the penetration depth of high-frequency eddy currents is much less than the ultrasonic wave length, the volumes forces, F_z and F_r, can be integrated with respect to the depth to obtain the surface forces, P_z and P_r.

The component P_z produces mainly longitudinal waves, but a small amount of radially polarized transverse waves arises from the restraining influence of the stress-free surface.[11-14] Similarly, P_r produces mainly radially polarized transverse waves, along with a small amount of longitudinal waves due to the surface restraints.[11,14] In this report an electromagnet is designed to produce large P_z and small P_r so as to make larger amplitude longitudinal waves and smaller amplitude radially polarized transverse waves. Ultrasonic waves that reflect from the sample backside are detected by a pickup coil through an exactly reversed phenomenon. The calculation of these fields is described further in the Appendix of this report.

---

[12]R. L. Roderick and R. Truell, "The Measurement of Ultrasonic Attenuation in Solids by the Pulse Technique and Some Results in Steel," *J. Appl. Phys.* 23(2): 267–79 (February 1952).

[13]F. Miller and H. Pursey, "The Field and Radiation Impedance of Mechanical Radiators on the Free Surface of a Semi-Infinite Isotropic Solid," *Proc. R. Soc. London Ser. A.*, 223: 521–41 (1954).

[14]Katsuhiro Kawashima, *The Theory and Numerical Calculation of the Acoustic Field Exerted by Eddy-Current Forces*, ORNL-5065 (in preparation).

Experimental Method

The transducer, shown in Fig. 2, consists of a big electromagnet to provide a stationary magnetic field, a small driver coil for generating eddy currents, and a small pickup coil. In this work, the radial component of magnetic flux near the steel pole pieces was between 5 and 2.5 kG, depending on the specific point, and the vertical component was between 4 and −1 kG; these results are from Fig. A1 in the Appendix of this report.

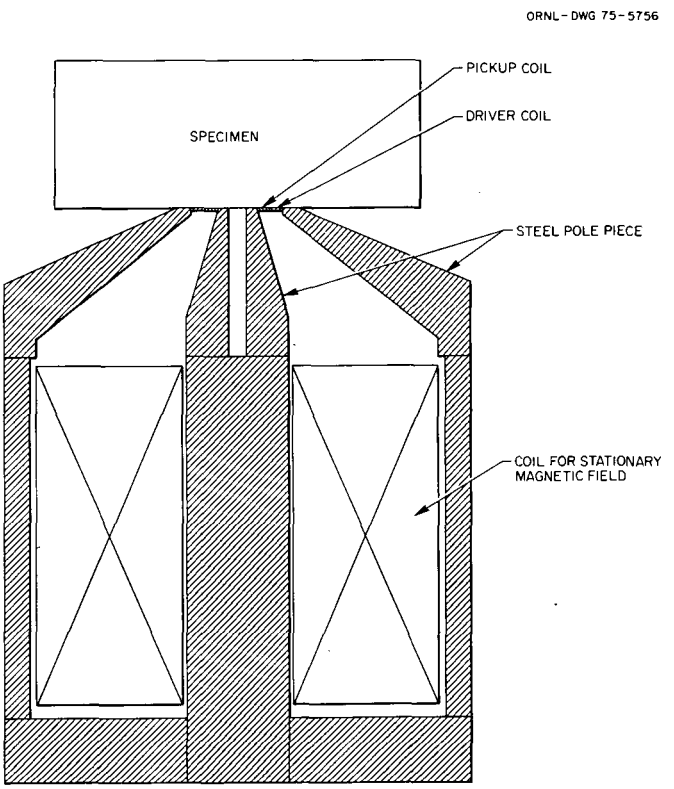

Fig. 2. Electromagnetic Transducer.

The pickup coil was located coaxially inside the driver coil because (1) the peak intensity of the longitudinal wave is on-axis and thus the pickup coil of smaller diameter detects it more efficiently; (2) coupling efficiencies between the coils and the specimen are better in this way because both coils can be located very near the specimen. The dimensions of the coils are as follows:

	Driver Coil	Pickup Coil
Dimensions, mm		
Outer radius	15	10
Inner radius	10	7.5
Thickness, including insulators	0.8	0.8
Number of turns	8	150

Method of Operation

A spark gap is used to make high-frequency pulse currents of high peak intensity in the driver coil. The pulse repetition rate is very low (0.3—2 pulses/sec). A capacitance (0.015 μF) is charged by a dc high-voltage power supply (19 kV) through a large resistance (40 MΩ). When a voltage breakdown occurs in the spark gap, a resonance circuit consisting of the capacitor, the driver coil, and a resistance (0.095 Ω) is formed, and a large pulse of high-frequency current runs through the circuit. The current is estimated by measuring a voltage difference across the 0.095-Ω resistance. The ultrasonic signal detected by the pickup coil is amplified and displayed on a cathode-ray tube. A picture is taken by a Polaroid camera. (See Fig. 3.)

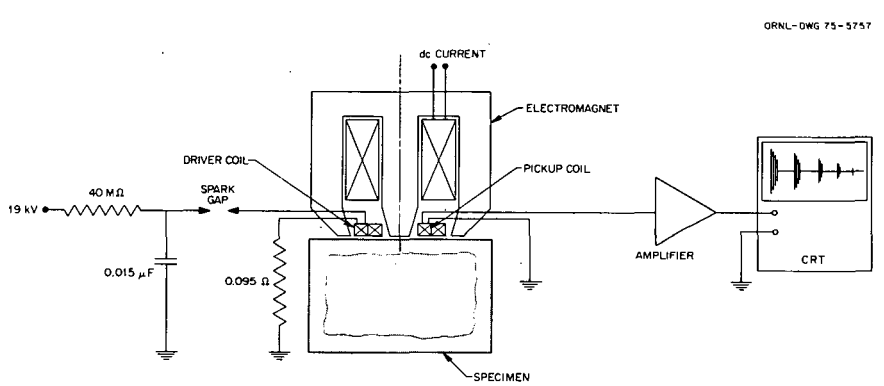

Fig. 3. Block Diagram of Apparatus.

Samples

Table 1 describes the six different samples tested. The mild steel and one of the aluminum samples are slabs large enough to avoid side reflections of the ultrasound. The other four specimens had artificial flaws drilled in the backside with an end mill to between one-fourth and one-third the sample thickness.

All the samples were tested by the same transducer under the same conditions with these exceptions: (1) the amplification factor was varied, (2) extra spacers were used to introduce vertical displacement between

the coil and the specimen in experiments run to determine the effect of such displacement, and (3) horizontal displacement was varied in experiments run to determine its effect.

Table 1. Samples

Sample	Material	Dimensions, mm		Flaw Characteristics, mm	
		Thickness	Diameter	Distance from Front	Diameter
1	Type 304 stainless steel	82.3	52.6	58.3	3.5
2	Type 304 stainless steel	73.5	52.6	59.1	1.3
3	Mild steel (ferromagnetic)	55.8	large	no flaw	
4	Aluminum	118.1	50.9	80.7	3.5
5	Aluminum	118.2	50.9	85.8	2.1
6	Aluminum	76.7	large	no flaw	

Driver Coil Current

The peak value of the driver current was between 1790 and 2320 A, and the frequency was between 1.4 and 1.7 MHz depending upon the different electrical and magnetic characteristics of each material (see Table 2). The ultrasonic waves generated have the same frequencies.

Table 2. Driver Coil Currents

Samples	Material	Frequency (MHz)	Peak Value of Current (A)
1,2	Type 304 stainless steel	1.6	1790
3	Mild steel	1.4	1890
4,5,6	Aluminum	1.7	2320

EXPERIMENTAL RESULTS

Determination of the Basic Characteristics of the Transducer

Samples 3 (mild steel) and 6 (aluminum) were tested first to find the characteristics of the transducer. These two samples were suitable for this purpose because they contain no flaws and are so wide that no side wall effects are expected. Figures 4 and 5 show the ultrasonic

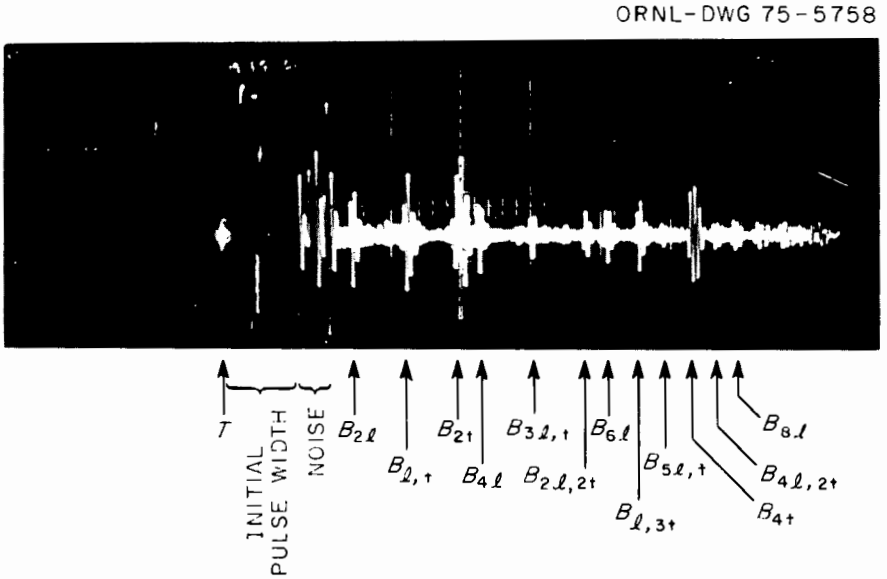

Fig. 4. Ultrasonic Reflections Obtained in Mild Steel (Sample 3) with the Electromagnetic Transducer. Frequency, 1.4 MHz; amplification, 830×; time base, 10.4 μsec/div; amplitude scale, 5 V/div.

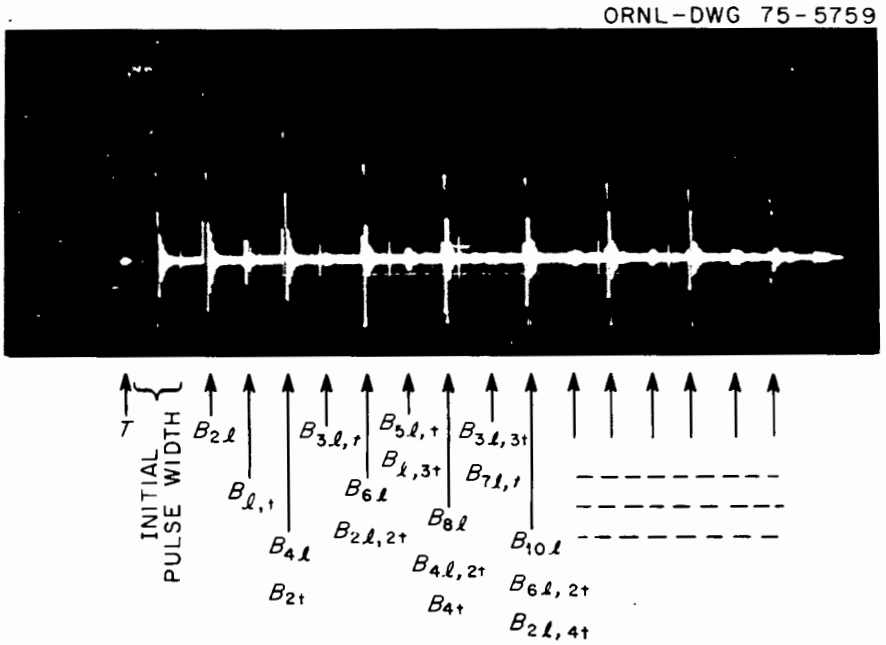

Fig. 5. Ultrasonic Reflections Obtained in Aluminum (Sample 6) with the Electromagnetic Transducer. Frequency, 1.7 MHz; amplification 107×; time base, 21.1 μsec/div; amplitude scale, 5 V/div.

signals generated in these specimens. In Fig. 4 there are several echoes that seem randomly distributed at first look. In Fig. 5 there are regularly spaced echoes and small extra echoes in between, except for the time period between the initial pulse (T) and the first bottom echo ($B_{2\ell}$). All the echoes of both Figs. 4 and 5 are explained by the following assumptions: (1) Both longitudinal and radially polarized transverse waves are generated and detected by the transducer. (2) Mode conversion between longitudinal and radially polarized transverse waves occurs at each reflection.

The signals for the mild steel sample are analyzed in Fig. 6. The first signal, $B_{2\ell}$, consists of only the longitudinal wave, and it is detected at time $t = 2t_\ell = 2L/C_\ell$ (C_ℓ is the longitudinal wave velocity and L is the sample thickness). The second signal, $B_{\ell,t}$, comprises two components: a radially polarized transverse wave, which is produced from the longitudinal wave through mode conversion at the back of the sample, and the longitudinal wave that is produced there from the transverse wave through mode conversion. Signal $B_{\ell,t}$ is detected at $t = t_\ell + t_t = t_t + t_\ell = L/C_\ell + L/C_t$ (C_t is the transverse wave velocity). The remaining echoes are explained similarly with reference to Fig. 6 and Table 3. The table gives the echo times measured on Fig. 4 and compares them with times calculated from

$$t = n_\ell t_\ell + n_t t_t \ , \tag{1}$$

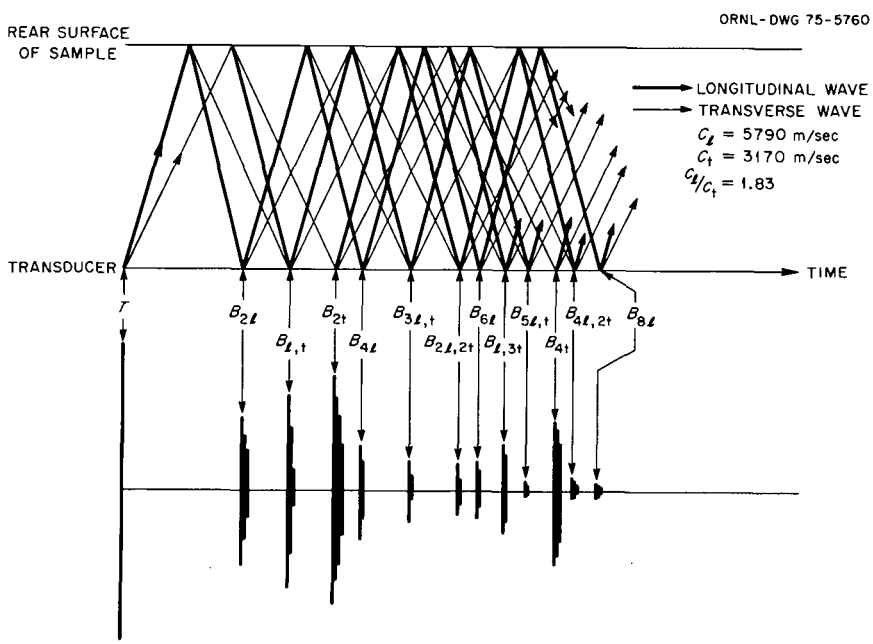

Fig. 6. Time Table for Reflections in Sample 3 (Mild Steel).

Table 3. Timing of Echoes in Sample 3 — Mild Steel

Time	Possible Different Paths	Echo	Relative Echo Time	
			Measured on Fig. 4	Calculated
	One Round Trip			
$2t_\ell$	$t_\ell + t_\ell$	$B_{2\ell}$	1.00	1.00
$t_\ell + t_t$	$t_\ell + t_t$, $t_t + t_\ell$	$B_{\ell,t}$	1.43	1.42
$2t_t$	$t_t + t_t$	B_{2t}	1.83	1.83
	Two Round Trips			
$4t_\ell$	$t_\ell + t_\ell + t_\ell + t_\ell$	$B_{4\ell}$	1.99	2.00
$3t_\ell + t_t$	$t_\ell + t_\ell + t_\ell + t_t$ $t_\ell + t_\ell + t_t + t_\ell$ $t_\ell + t_t + t_\ell + t_\ell$ $t_t + t_\ell + t_\ell + t_\ell$	$B_{3\ell,t}$	2.41	2.42
$2t_\ell + 2t_t$	$t_\ell + t_\ell + t_t + t_t$ $t_\ell + t_t + t_t + t_\ell$ $t_\ell + t_t + t_\ell + t_t$ $t_t + t_t + t_\ell + t_\ell$ $t_t + t_\ell + t_\ell + t_t$ $t_t + t_\ell + t_t + t_\ell$	$B_{2\ell,2t}$	2.85	2.83
$t_\ell + 3t_t$	$t_\ell + t_t + t_t + t_t$ $t_t + t_\ell + t_t + t_t$ $t_t + t_t + t_\ell + t_t$ $t_t + t_t + t_t + t_\ell$	$B_{\ell,3t}$	3.26	3.25
$4t_t$	$t_t + t_t + t_t + t_t$	B_{4t}	3.67	3.66
	Three Round Trips			
$6t_\ell$	$t_\ell + t_\ell + t_\ell + t_\ell + t_\ell + t_\ell$	$B_{6\ell}$	3.01	3.00
$5t_\ell + t_t$	6 different paths	$B_{5\ell,t}$	3.43	3.42
$4t_\ell + 2t_t$	15 different paths	$B_{4\ell,2t}$	3.84	3.83
4 other times	42 different paths			
	Four Round Trips			
$8t_\ell$	$t_\ell + t_\ell + t_\ell + t_\ell + t_\ell + t_\ell + t_\ell + t_\ell$	$B_{8\ell}$	3.99	4.00
8 other times	255 different paths			
	***n* Round Trips**			
$(2n + 1)$ different times	2^{2n} different paths			

where t_ℓ and t_t are obtained from the measured times of $B_{2\ell}$ and B_{2t}, respectively, and n_ℓ and n_t are the numbers of one-way paths in the respective modes.

An echo that completes n round trips ($2n = n_\ell + n_t$) may be detected at $2n + 1$ different times, as given by Eq. (1), and may take 2^{2n} different combinations of paths. Examples for all echoes that complete one or two round trips and some that complete three or four are shown in Table 3. Table 3 shows that many echoes can exist, and the number of echoes increases rapidly with the increase in the number of round trips. This is why many echoes appear at the longer times.

In the case of aluminum, several echoes come almost at the same time and produce an apparently simpler picture. This is because the ratio of the longitudinal to the transverse wave velocity is very slightly greater than 2 for aluminum. (See Figs. 5 and 7.)

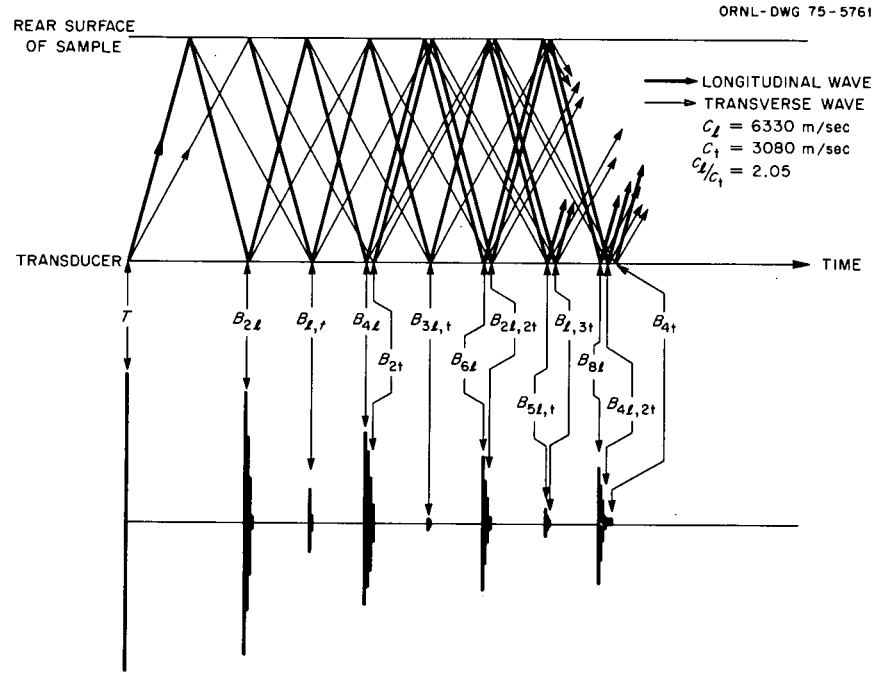

Fig. 7. Time Table for Reflections in Sample 6 (Aluminum).

The transducer is designed to give a better efficiency for the longitudinal wave than for the radially polarized transverse wave. (See the magnetic flux distribution in Fig. A1.) However in the case of a ferromagnetic material the magnetic flux shown in Fig. A1 is greatly changed, to make a larger vertical than horizontal component very close to the specimen surface, where the ultrasonic waves are generated and detected. Consequently, the efficiency for detecting a radially polarized transverse wave becomes greater than that for a longitudinal wave. This is probably why B_{2t} is larger than $B_{2\ell}$ in Fig. 4. Magnetostriction is also considered to contribute to the different characteristics of the transducer for ferromagnetic material.

The mode conversion between longitudinal and radially polarized trasnverse waves will be considered in detail later in this report.

Flaw Detection

Two pieces of stainless steel (samples 1 and 2) and two pieces of aluminum (samples 4 and 5) were tested to examine the flaw detection ability of the electromagnetic transducer. The samples were also tested by a commercial ultrasonic nondestructive test instrument with a ceramic transducer (2.25 MHz, 25.4 mm diam). The instrument used is considered to be representative of good instruments commercially available.

Sample 1 (type 304 stainless steel) has a fairly large artificial flaw (3.5-mm-diam drilled hole) in it (see Table 1). The test results with the electromagnetic transducer are shown as Fig. 8(a). Echo F_1 is from the flaw; $B_{2\ell}$ and $B_{\ell,t}$ are back-surface echoes as defined in Table 3. We consider S_1 and S_2 to be back-surface echoes delayed through mode conversion at side walls of the sample and the drilled hole (flaw). In this case, the mode conversion occurs between the lontigudinal wave and linearly polarized transverse wave. The path of S_1 is considered to be 1-2-3-4-5 as shown in Fig. 9; S_2 is similarly considered to be 1-2-3-6-7-8. Such side reflections are well known in ultrasonic nondestructive testing.[15]

The angle α is calculated approximately from

$$\alpha = \sin^{-1} (C_t/C_\ell) \ , \tag{2}$$

and the delayed echo times by

$$S_1 = \frac{2L}{C_\ell}\left[1 + \frac{d - d_f}{4L}\sqrt{(C_\ell/C_t)^2 - 1}\right] \ , \tag{3}$$

$$S_2 = \frac{2L}{C_\ell}\left[1 + \frac{d - d_f}{2L}\sqrt{(C_\ell/C_t)^2 - 1}\right] \ , \tag{4}$$

where L = sample length, d = sample diameter, and d_f = flaw diameter. The results calculated with Eqs. (3) and (4) agree very well with the results measured on Fig. 8. Sample 1 was also tested with the ceramic transducer, and the result is shown in Fig. 8(b) without rectification

---

[15] J. Krautkrämer and H. Krautkrämer, *Ultrasonic Testing of Materials*, Springer-Verlag, New York, 1969.

ORNL-DWG 75-5762

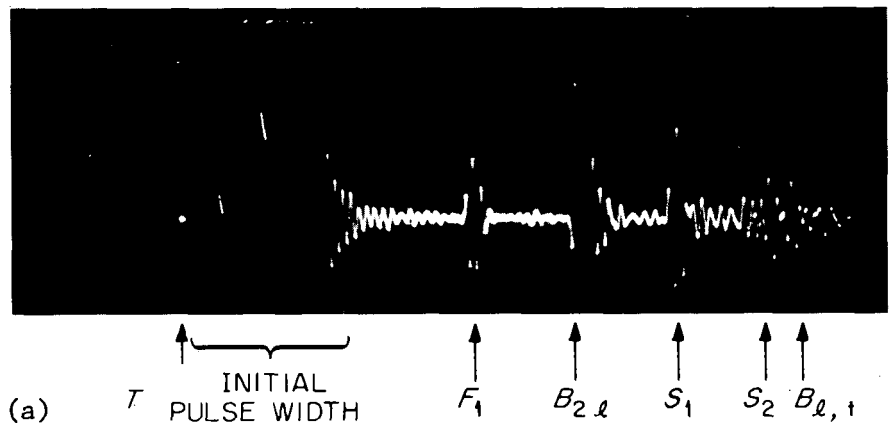

ORNL-DWG 75-5763

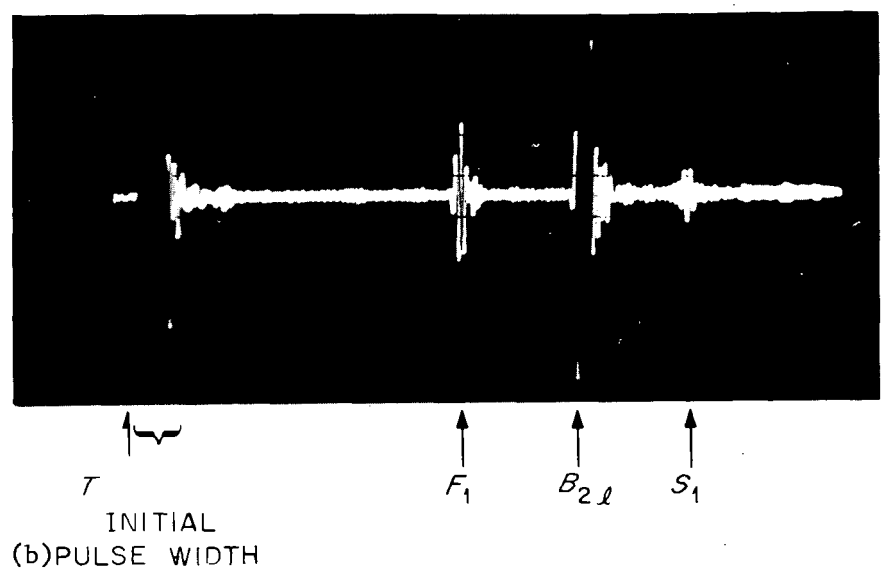

Fig. 8. Ultrasonic Echoes in Type 304 Stainless Steel Sample 1 — 82.3 mm Thick by 52.6 mm in Diameter, 3.5-mm-diam Flaw Drilled to 58.3 mm from Front Surface. (a) Observed with electromagnetic transducer with 960× amplification, 5 V amplitude, 5.2 μsec/div time base, 1.6 MHz. (b) Observed with ceramic transducer, 2.25 MHz, 25.4 mm in diameter.

ORNL-DWG 75-5768

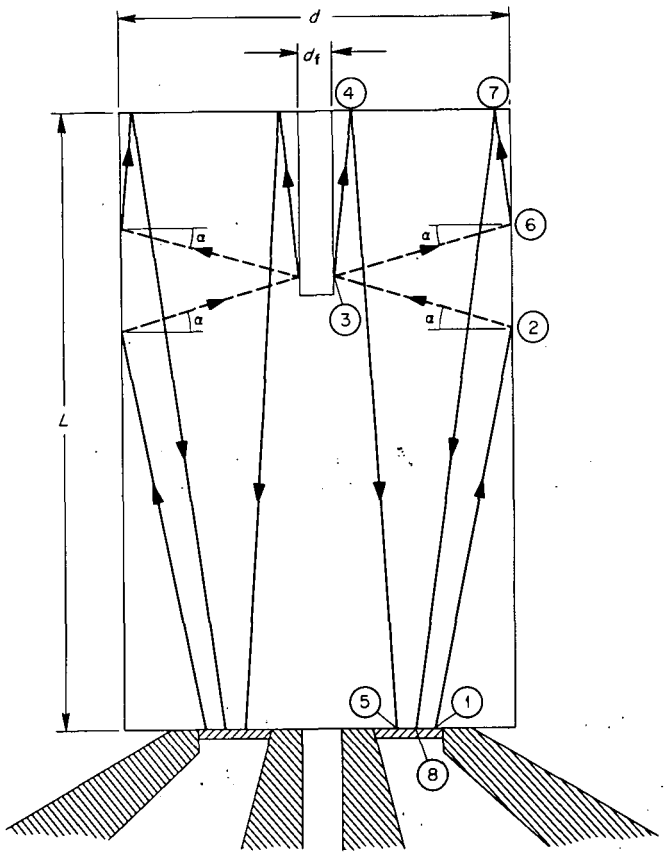

Fig. 9. Paths of Delayed Back-Surface Echoes S_1 and S_2 in Sample 1. Echo S_1 arises from path 1-2-3-4-5; S_2 from 1-2-3-6-7-8.

for better comparison of the signal-to-noise ratio with that of the electromagnetic transducer, because true information about the signal-to-noise ratio is sometimes lost in the video mode. The echoes F_1, $B_{2\ell}$, and S_1 are the same as shown in Fig. 8(a).

Sample 2 (type 304 stainless steel) was also tested by the electromagnetic and ceramic transducers, and Fig. 10 shows the echo patterns. Results with both transducers for type 304 stainless steel are compared in Table 4. Both showed a good signal-to-noise ratio.

The method of comparison is not perfect because the diameter and the frequencies are not the same for both transducers. However we can obtain some idea of the ability of the electromagnetic transducer through this comparison. We can say that the signal-to-noise ratio of the electromagnetic transducer is as good as that of the ceramic transducer as far as this experiment is concerned. Especially, the electromagnetic transducer detected a small flaw (1.3 mm diam) in sample 2 (type 304 stainless steel) very clearly [see Fig. 10(a)]. This is considered to be very good sensitivity for an electromagnetic transducer because the efficiency of an electromagnetic transducer is considered to be greatly affected by the electrical conductivity of a sample. Most of the previously

ORNL-DWG 75-5769

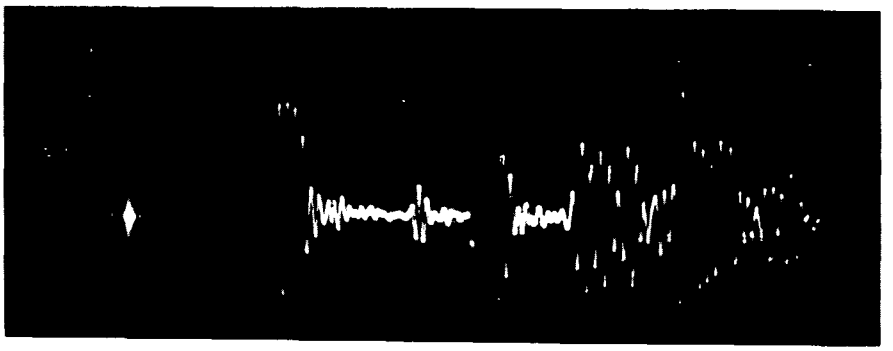

(a) INITIAL PULSE WIDTH F_1 $B_{2\ell}$ S_1 S_2 $B_{4\ell}$

ORNL-DWG 75-5770

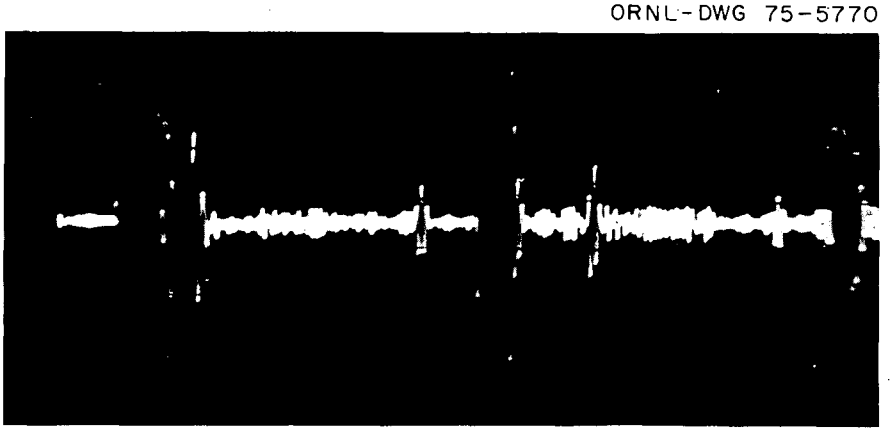

(b) INITIAL PULSE WIDTH F_1 $B_{2\ell}$ S_1 F_2 $B_{4\ell}$

Fig. 10. Ultrasonic Echoes in Type 304 Stainless Steel Sample 2 — 73.5 mm Thick by 52.6 mm in Diameter, 1.3-mm-diam Flaw Drilled to 59.1 mm from Front Surface. (a) Observed with electromagnetic transducer with 960× amplification, 2 V/div amplitude, 5.2 μsec/div time base, 1.6 MHz (b) Observed with ceramic transducer, 2.25 MHz, 25.4 mm in diameter.

Table 4. Comparison Between Electromagnetic and Ceramic Transducers Tested on Type 304 Stainless Steel

Transducer	Diameter (mm)	Frequency (MHz)	Front Dead Zone	Echoes After $B_{2\ell}$
Electromagnetic	Driver coil (OD) 30 Pickup coil (OD) 20	1.6	large	many
Ceramic	25.4	2.25	small	few

reported work on electromagnetic transducers has dealt only with good electrical conductors like aluminum. The good efficiency of the electromagnetic transducer reported here is due to (1) high pulse current in the driver coil (peak value about 2000 A) and (2) a large number of turns (150) in the pickup coil. A front dead zone arising from the initial pulse width is very large (e.g., 25 mm for stainless steel), which is one of the disadvantages of an electromagnetic transducer.

Samples 4 (aluminum, flaw diameter 3.5 mm) and 5 (aluminum, flaw diameter 2.1 mm) were also tested, and Fig. 11 shows the echoes observed. Echoes T, F_1, $B_{2\ell}$, and S_1 correspond to analogous echoes in the stainless steel samples. Echoes X_1, X_2, and X_3 are not fully explained, but we can say that they are associated with the artificial flaw because they do not appear in the absence of a flaw.

Effect of Transducer-to-Specimen Spacing

The relative changes of echo amplitude due to increased distance between the sample and the transducer were tested for stainless steel sample 1. Added distances were 0.38 and 0.76 mm. The echo patterns observed with these spacers are shown in Fig. 12; the corresponding pattern without the spacers in Fig. 8(a). The relative amplitudes of the echoes are plotted in Fig. 13. As expected, the amplitudes of F_1, $B_{2\ell}$, and S_1 all decrease at almost the same rate with distance. The decrease ratio is represented approximately by $\exp(-1.6h)$, where h is the distance in millimeters between the specimen and the transducer This decrease is not as sharp as had been expected. This makes the electromagnetic transducer favorable in many respects.

Effect of Horizontal Displacement

The effects of horizontal displacement of the transducer and sample 1 were examined for displacements from 1.27 through 5.08 mm.

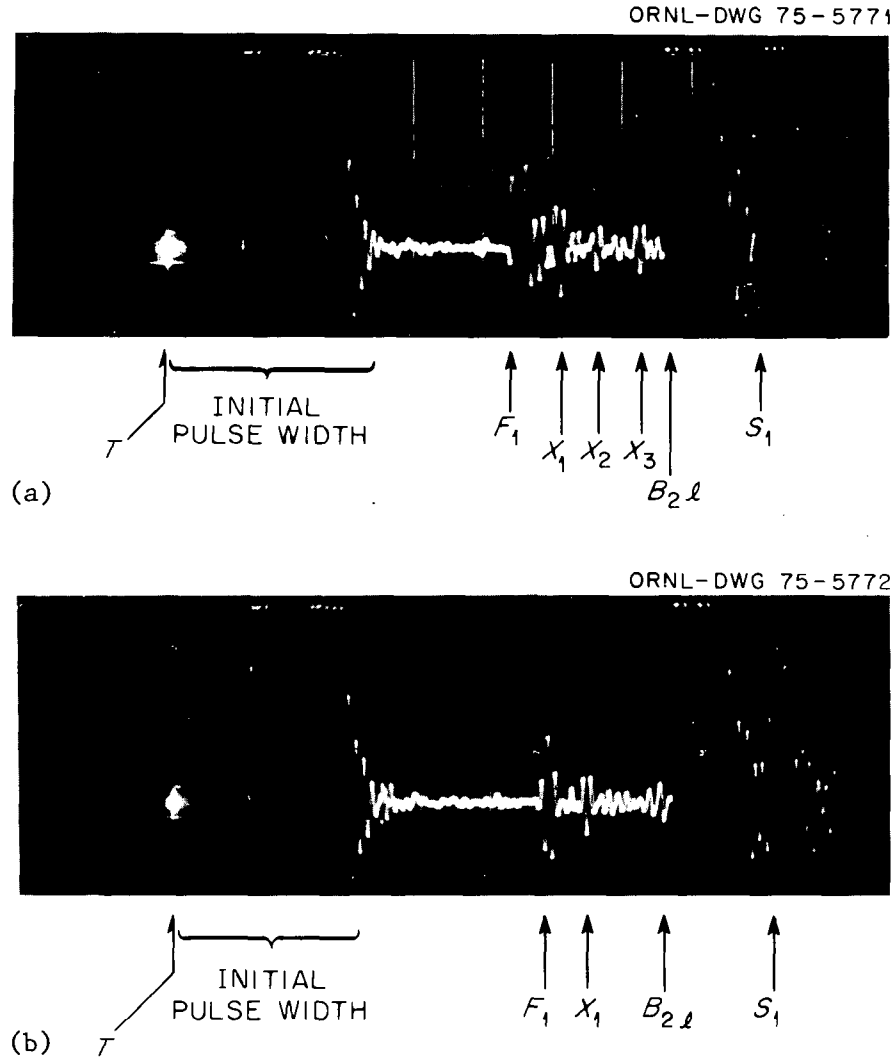

Fig. 11. Ultrasonic Echoes Observed in Aluminum with the Ultrasonic Transducer. Amplification, 1100×; time base, 5.2 μsec/div; amplitude, 5 V/div; frequency 1.7 MHz. (a) Sample 4, 118.1 mm thick by 50.9 mm diam, 3.5-mm-diam flaw 80.7 mm from front surface. (b) Sample 5, 118.2 mm thick by 50.9 mm diam, 2.1-mm-diam flaw 85.8 mm from front surface.

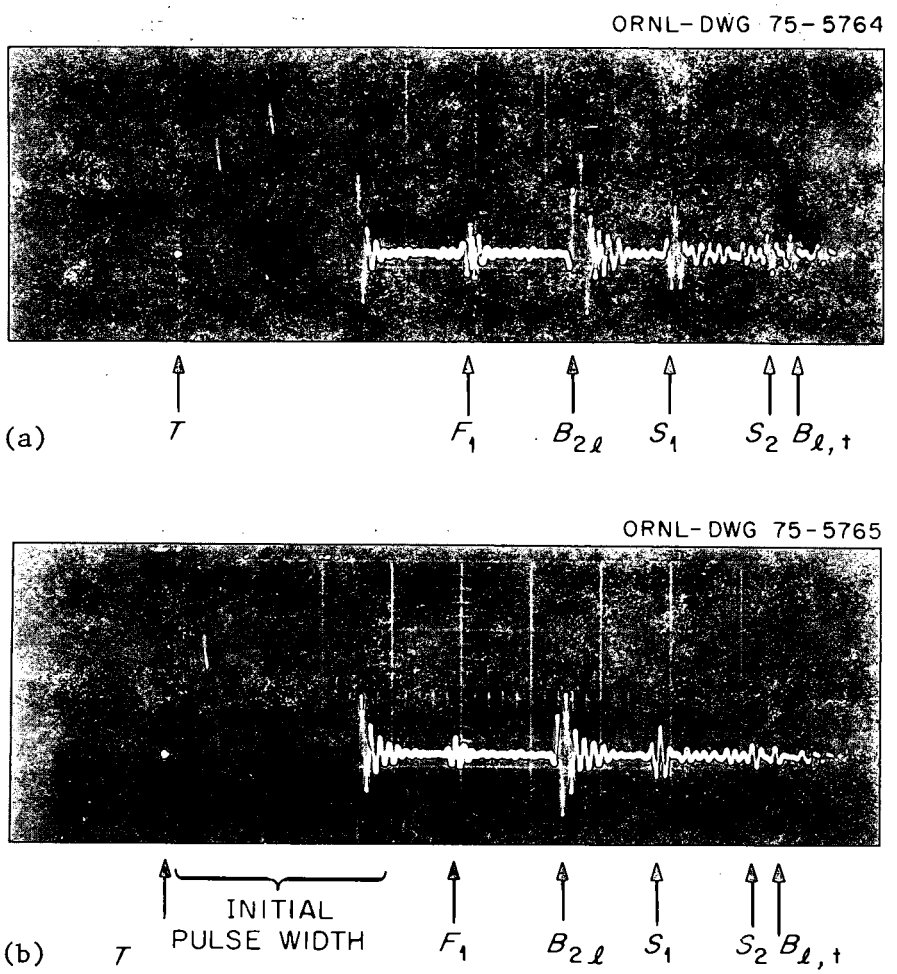

Fig. 12. Effect of Added Spacers on the Echo Patterns Observed in Type 304 Stainless Steel Sample 1 with the Electromagnetic Transducer. (a) 0.38 mm spacer added. (b) 0.76 mm spacer added.

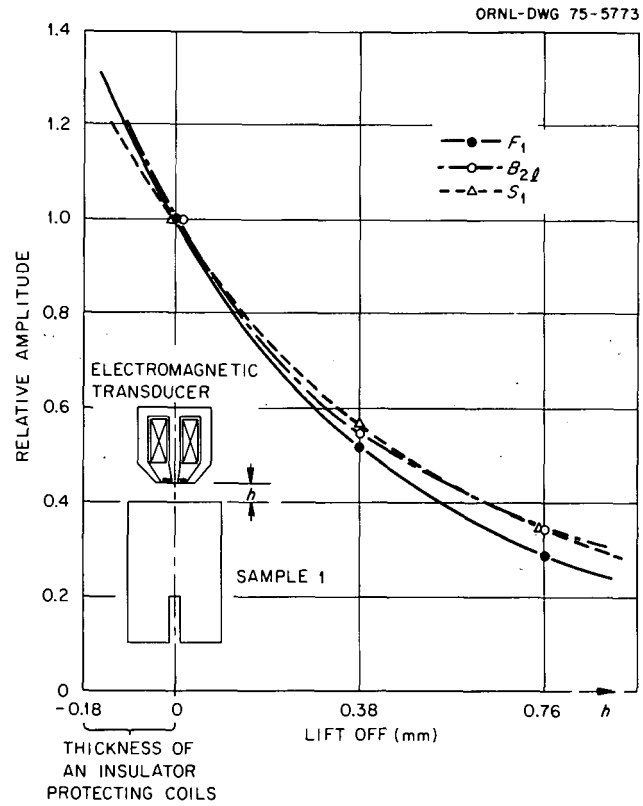

Fig. 13. Variation of Echo Amplitudes with Distance Between Electromagnetic Transducer and Type 304 Stainless Steel Sample 1.

Figure 14 shows the echo patterns, and Fig. 15 shows the variation of relative amplitudes of the echoes with displacement. Echo F_1 decreases more rapidly than was expected from the size of the transducer (driver coil 30 mm diam, pickup coil 20 mm diam). This shows that the ultrasonic wave beam produced by the electromagnetic transducer is very sharp, which is also shown in the calculated ultrasonic field in the Appendix of this report (see Fig. A6). In Fig. 15 S_1 also decreases, as is expected because the side walls of a sample and a drill hole lose symmetry with respect to the axis of the ultrasonic wave when a horizontal displacement increases. The slight increase of $B_{2\ell}$ is considered to be due to the recovery of some of ultrasonic wave energy that is interrupted from reaching the bottom by the drilled hole when the axes of the ultrasonic wave beam and the flaw coincide.

Wave Velocity Measurement

The longitudinal and transverse wave velocities were obtained by measuring the timing of the echoes ($B_{2\ell}$, $B_{\ell,t}$, B_{2t}, ... etc.) on the photographs. Several photographs for each material were used to obtain an average measurement. Not all the photographs used are shown in this report. The results are shown in Table 5.

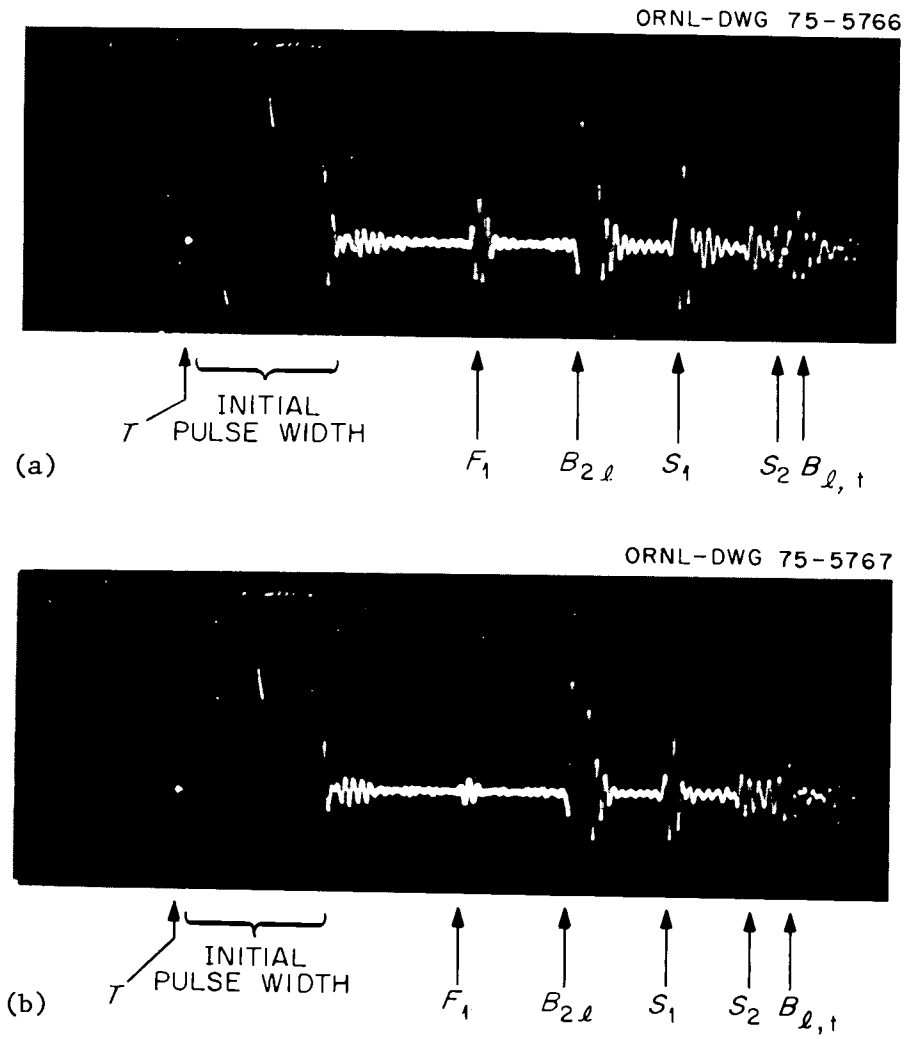

Fig. 14. Effect of Horizontal Displacement on the Echo Patterns Observed in Type 304 Stainless Steel Sample 1 with the Electromagnetic Transducer. (a) 2.54 mm displacement. (b) 5.08 mm.

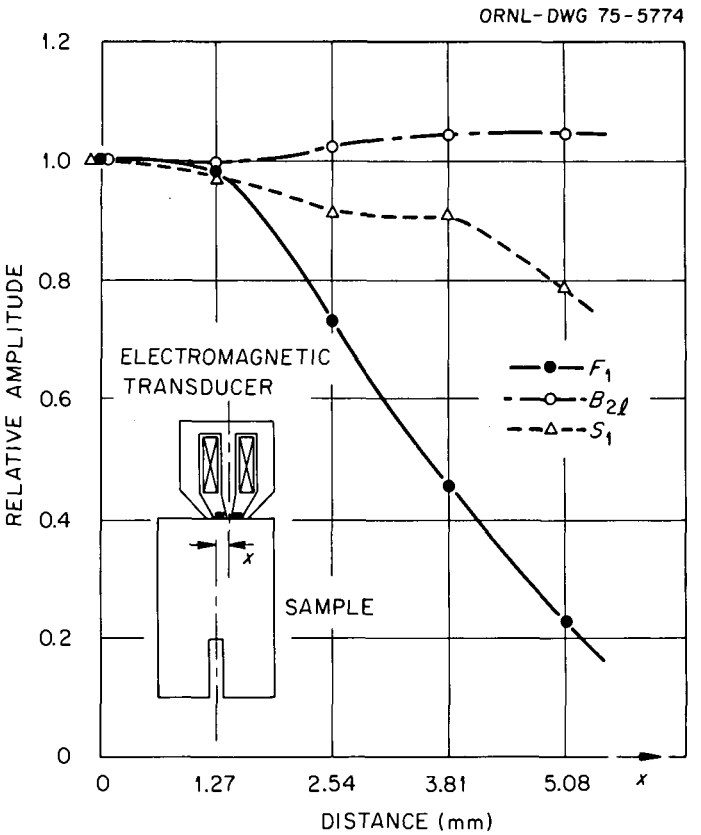

Fig. 15. Relative Changes of Signal Amplitudes Due to Increased Horizontal Displacements Between the Transducer and the Sample.

Table 5. Ultrasonic Wave Velocities Measured by the Electromagnetic Transducer

Material	Wave Velocity, m/sec	
	Longitudinal	Transverse
Type 304 stainless steel	5630	2690
Mild steel	5790	3170
Aluminum	6330	3080

CONSIDERATIONS OF THE MODE CONVERSION

Echo signals similar to those in Figs. 4 and 5 have already been observed with conventional piezoelectric transducers.[16-18] However none of the reports properly explained the phenomenon.

The mode conversion between a longitudinal wave and a radially polarized wave is very different from the mode conversion between a longitudinal wave and a linearly polarized transverse wave. Figure 16 (sample 6, aluminum), shows that the mode conversion efficiency between a longitudinal wave and a radially polarized transverse wave is fairly large even at reflections with very small incident angles. The meanings of $B_{38\ell}$, $B_{37\ell,t}$, $B_{40\ell}$, $B_{39\ell,t}$, $B_{42\ell}$, etc. can be inferred from Table 3. For example, $B_{43\ell,t}$ is detected by the pickup coil as a radially polarized transverse wave that is produced from a longitudinal wave, $B_{43\ell}$, through mode conversion at the last reflection at the sample back surface. The incident angle of the longitudinal wave, $B_{43\ell}$, at the sample bottom must be less than θ (see Fig. 17), given by

$$\theta = \tan^{-1} r/44L = \tan^{-1} \frac{10 \text{ mm}}{44 \times 76.7 \text{ mm}} \approx 0.17° ,$$

where L = sample thickness,
r = outer radius of pickup coil.

Mode conversion efficiency for the incident angle θ ($\approx 0.17°$) using the assumption of a plane wave is extremely small (less than 2.9×10^{-3}, in this case), which can definitely not explain the fairly large amplitudes of $B_{37\ell,t}$, $B_{39\ell,t}$, $B_{41\ell,t}$, and $B_{43\ell,t}$ in Fig. 16, because the detecting efficiency of the pickup coil for a radially polarized transverse wave cannot be greater than the efficiency for a longitudinal wave by a large factor (for example, as large as $1/2.9 \times 10^{-3} \approx 300$).

The restraint by the solid surface and the sharpness of the ultrasonic beam lead us to the following simple considerations that help us to understand the mode conversion between a longitudinal wave and a radially polarized transverse wave. When a longitudinal wave that has an axially symmetric intensity distribution arrives at a boundary [see Fig. 18(a)], it deforms the boundary. A point A on the boundary is displaced not only vertically but also horizontally by this deformation. Horizontal displacements

---

[16] J. Krautkrämer and H. Krautkrämer, *Ultrasonic Testing of Materials*, Springer-Verlag, New York, 1969.

[17] W. Grabendörfer and J. Krautkrämer, "Impuls-Echo-Prüfung on Plattenförmigen Korpern," *Z. Metallk.* 49: 22–26 (1958).

[18] M. A. Kassem, "Echo-Phantoms," *Iron Steel Int.* 29(12): 503–9 (1956).

ORNL-DWG 75-5782

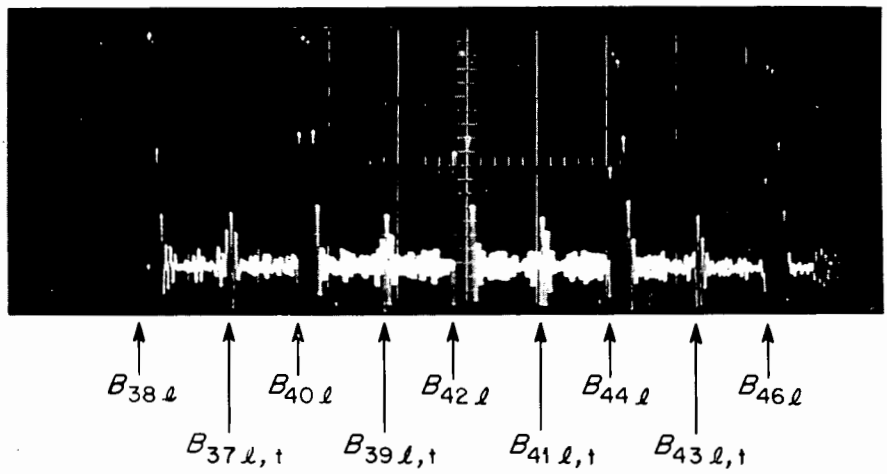

Fig. 16. High-Order Reflections Observed in Aluminum (Sample 6) with the Electromagnetic Transducer. Note prominence of echoes with one transverse crossing, showing importance of mode conversion even at very low angles of incidence. Amplification 1000×, time base 10.4 μsec/div, amplitude 5 V/div.

ORNL-DWG 75-5783

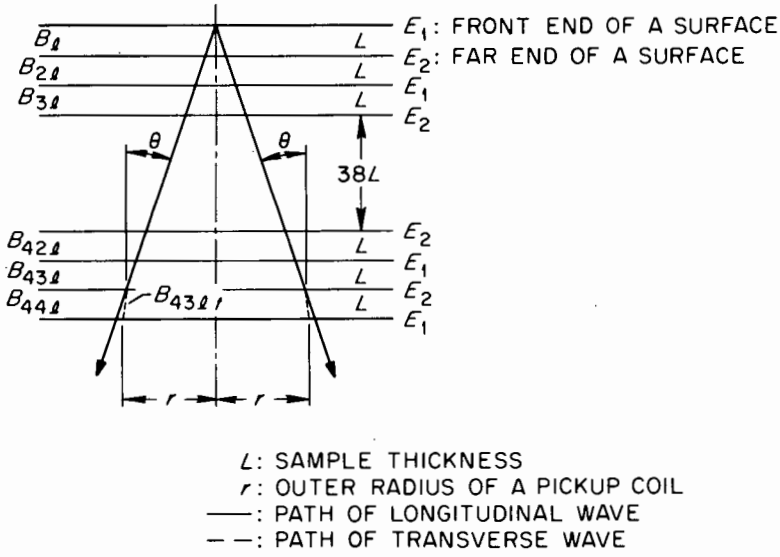

Fig. 17. Path of Echo $B_{43\ell,t}$.

ORNL-DWG 75-5784

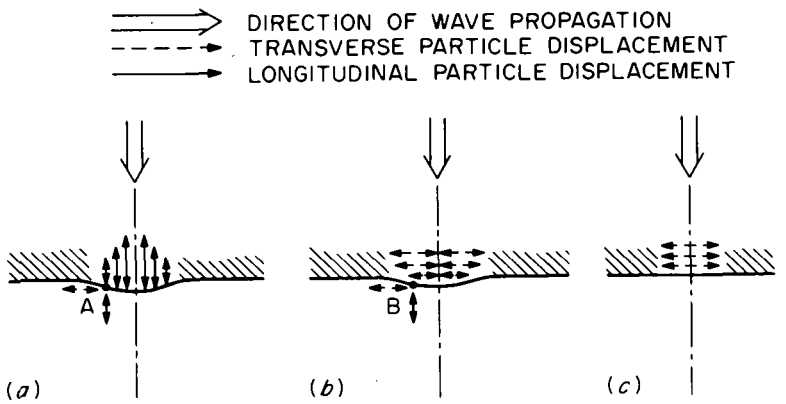

Fig. 18. Interactions of Incident Beams of Ultrasound with Surface, Showing Possibility of Mode Conversion. (a) Incident longitudinal wave produces lateral compression, generating radially polarized transverse wave. (b) Lateral restraint of vibrations from incident radially polarized transverse wave sets up longitudinal vibrations in reflected wave. (c) Vibrations of incident linearly polarized transverse wave are not restrained, so no mode conversion occurs.

distribute symmetrically around the axis, producing a radially polarized transverse wave. When a radially polarized transverse wave arrives at a boundary [see Fig. 18(b)] and causes a radial horizontal displacement, some of the material is squeezed out vertically because the material can not shrink infinitely. Consequently, a point, B, on the boundary is displaced not only horizontally, but also vertically, and some longitudinal wave is generated. When a linearly polarized transverse wave arrives vertically [see Fig. 18(c)] at a boundary and causes a horizontal displacement, no vertical displacement occurs because a one-direction horizontal displacement can be absorbed into the spreading material without causing any vertical displacement.

Very high sensitivity and special care are necessary for both a longitudinal wave and a radially polarized transverse wave to be detected by a piezoelectric transducer made for a longitudinal wave.[16-18] In the case of a conventional piezoelectric transducer, there is usually a liquid layer between the transducer and sample (see Fig. 19). Only longitudinal waves (ℓ_1) can travel through liquid. A longitudinal wave (ℓ_2) and a small amount of radially polarized transverse wave (t_2) are generated at the boundary of liquid and solid through mode conversion. At the far end of the solid, mode conversion occurs, and both waves (ℓ_3, t_3) are generated The longitudinal wave (ℓ_3) is detected easily as longitudinal wave (ℓ_4). but the radially polarized transverse wave (t_3) can be detected only as longitudinal wave (ℓ_5) after mode conversion at the boundary. Thus very high sensitivity and special care are necessary to detect ℓ_5, since its amplitude has been made smaller and smaller through several mode conversions and is too small to be detected by usual techniques.

ORNL-DWG 75-5785

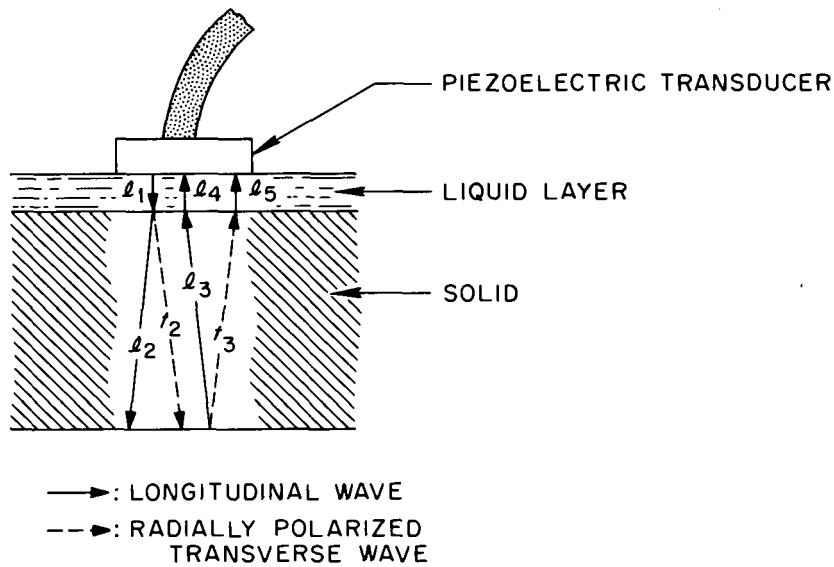

Fig. 19. Mechanism of Detecting Transverse Ultrasonic Waves with a Piezoelectric Transducer.

SUMMARY AND CONCLUSION

An electromagnetic transducer that generates and detects a relatively large amount of longitudinal ultrasonic wave and a small amount of radially polarized transverse ultrasonic wave was made and tested on stainless steel, mild steel, and aluminum. The flaw detection ability of the electromagnetic transducer is almost as good as that with a commercially available ceramic transducer. Finally, ultrasonic fields produced by the electromagnetic transducer were calculated, and the interaction between the longitudinal wave and a radially polarized transverse wave was also considered.

ACKNOWLEDGMENTS

The author would like to express his appreciation to R. W. McClung for his encouragement for this research work, for his review of this report and many helpful suggestions, to W. E. Deeds, C. V. Dodd, and S. Peterson for their review of this report and their many helpful suggestions, and to L. D. Chitwood for suggestions about constructing the coils. He would also like to acknowledge the help of Stephanie Davison in the typing of this report.

APPENDIX

Calculation of the Ultrasonic Wave Fields Produced by the Electromagnetic Transducer

The ultrasonic wave field produced in sample 1 (type 304 stainless steel) by the electromagnetic transducer used in this experiment was calculated by the method developed by the author.[1] The method is based on the following assumptions:

1. Ultrasound is generated by the electromagnetic force through classical and macroscopic phenomena.
2. The electric, magnetic, and elastic properties of the material are linear, isotropic, and homogeneous throughout the sample, which occupies semiinfinite space.

The electromagnetic force that is produced by an interaction of eddy currents and stationary magnetic fields is represented by the Lorentz formula:

$$\vec{F} = \vec{I} \times \vec{B} ,$$

which we can resolve into

$$F_z = I_\phi B_r , \tag{A1}$$

$$F_r = I_\phi B_z . \tag{A2}$$

The stationary magnetic flux produced by the electromagnet at the surface of a sample was measured by a Hall element. If a material is nonmagnetic, the magnetic flux is not changed by the presence of the material. The measured results are shown in Fig. A1. The horizontal and radial component, B_r, is relatively more constant and larger than the vertical component, B_z, at the locations of the driver and pickup coils, as is expected from the design of the electromagnet. Notice that B_z changes its sign at point C, where $B_z = 0$.

---

[1]Katsuhiro Kawashima, *The Theory and Numerical Calculation of the Acoustic Field Exerted by Eddy-Current Forces,* ORNL-5065 (in preparation).

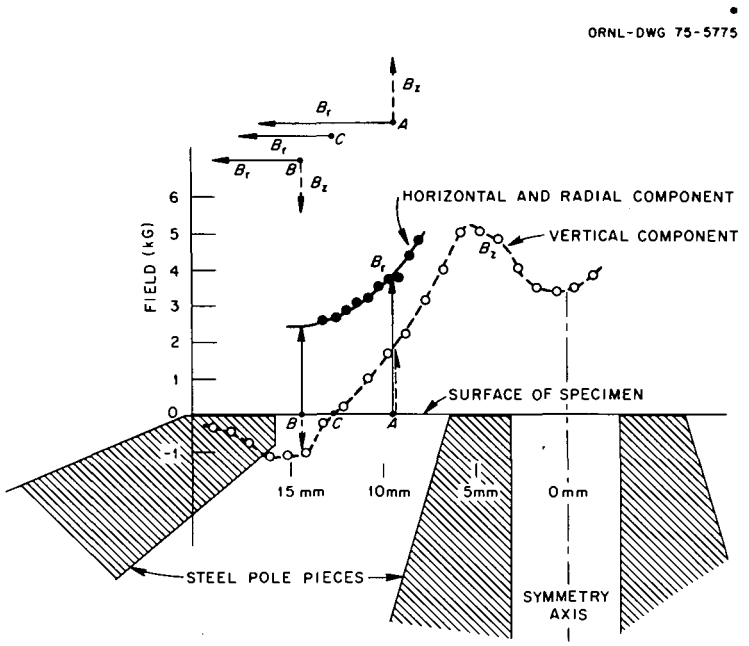

Fig. A1. Magnetic Flux at the Surface of a Nonmagnetic Sample.

The eddy current density is obtained by

$$\vec{I} = \sigma\vec{E}$$

$$= \sigma \frac{\partial\vec{B}}{\partial t}$$

$$= -\sigma \frac{\partial}{\partial t} (\nabla \times \vec{A}) ,$$

where $\vec{A}$ = vector potential of a coil, and
σ = electric conductivity of the material.

A rigorous method for calculating the vector potential of a coil shown in Fig. A2 was developed by Dodd and Deeds[2] and Onoe.[3] Coil dimensions,

[2]C. V. Dodd and W. E. Deeds, "Analytical Solutions to Eddy-Current Probe-Coil Problems," *J. Appl. Phys.* 39(6): 2829–38 (May 1967).

[3]M. Onoe, "An Analysis of a Finite Solenoid Coil Near a Conductor," *Denki Gakkai Zasshi*, 88(10): 1894–1902 (October 1968).

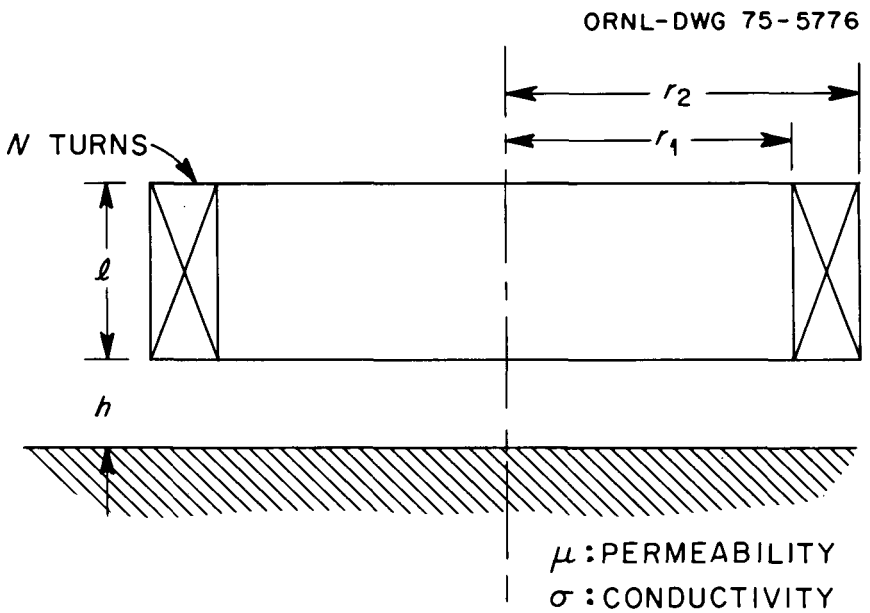

Fig. A2. Variables for the Calculation of the Vector Potential of a Coil at any Point.

driver current (1790 A), electrical conductivity (74 μΩ-cm for sample 1) and magnetic permeability ($4\pi \times 10^{-7}$ H/m for sample 1) are necessary for the calculation.

The calculation was made for sinusoidal currents with an amplitude equal to the peak value of the pulse current. The result can be considered as a good approximation for pulse currents as far as the peak value is concerned. The steel pole pieces are neglected in the calculation. They are not considered to have a great effect on the eddy-current distribution, because most of the turns of the driver coil are far from the steel pole pieces when they are very near the sample. The results of calculations, the eddy-current density at the sample surface and at a depth of 0.5 mm, are shown in Fig. A3. The maximum eddy-current density at a surface is about 1.15×10^{10} A/m^2, which is very large but smaller than the current density in the driver coil, about 3.6×10^{10} A/m^2. Notice that because of the skin effect, the eddy-current density decreases rapidly as the depth increases.

The force per unit volume is calculated by Eqs. (A1) and (A2), and the results are shown in Fig. A4. The vertical force, F_z, has its peak near the outer radius of the driver coil and decreases very rapidly toward both the outside and the inside of the driver coil. The horizontal and radial component of the force, F_r, has zero value and changes it phase at the point where the vertical component of the stationary magnetic flux has zero value. (See Figs. A1 and A4).

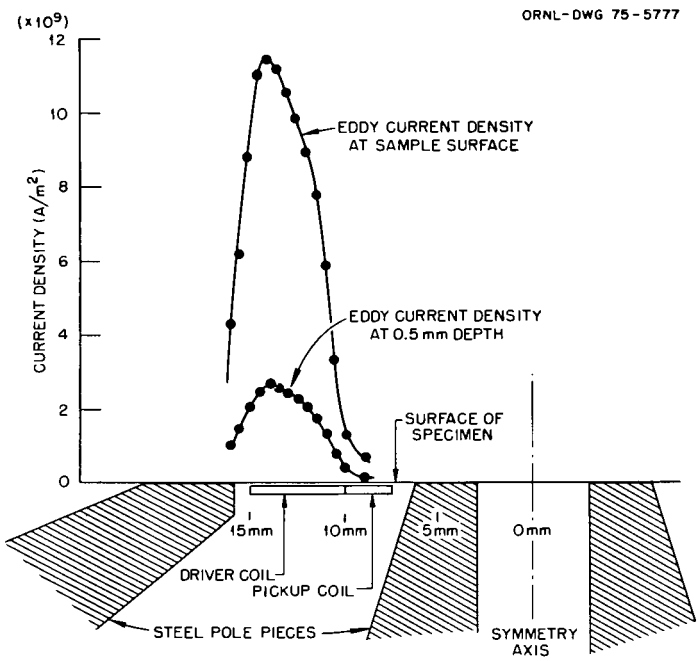

Fig. A3. Eddy-Current Density in Sample 1.

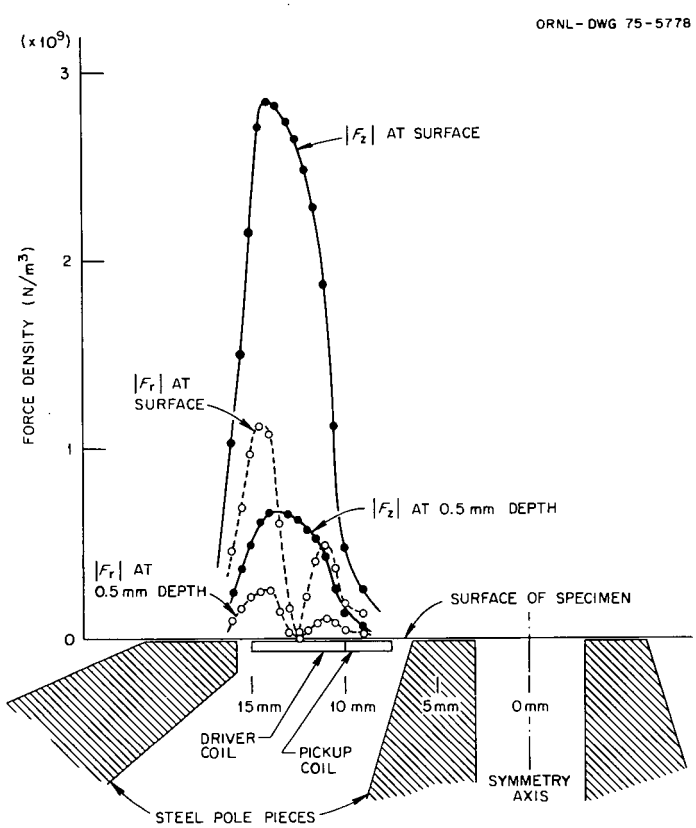

Fig. A4. Electromagnetic Force Per Unit Volume Produced in Sample 1 by the Electromagnetic Transducer.

The surface forces, P_z and P_r, which are obtained through integration of the volume forces with respect to the depth, are shown in Fig. A5. This is proper treatment of the forces if the skin depth of the eddy current is much less than the elastic wavelengths. In the case of sample 1 (type 304 stainless steel, where the electrical conductivity is 74 μΩ-cm, the longitudinal wave velocity is 5630 m/sec, the transverse wave velocity is 2690 m/sec, and the frequency is 1.6 MHz), the skin depth (about 0.34 mm) is not much less than the wavelengths (3.5 and 1.7 mm for longitudinal and transverse waves, respectively). Nevertheless, we use the surface force assumption for simplicity, knowing that some minor errors may come from it.

According to Figs. A4 and A5, the distribution of surface and volume forces is almost the same. The phase of the vertical surface force, $Ph(P_z)$, does not change much in the region where the amplitude, $|P_z|$, is large enough to contribute the main part of the ultrasonic field. The phase of the horizontal and radial surface force, $Ph(P_r)$, is the same as $Ph(P_z)$ if the signs are taken as positive for both the directions of depth increase and radius increase. $Ph(P_r)$ changes its value by π at the point where B_z changes its sign. (See Figs. A1 and A5.)

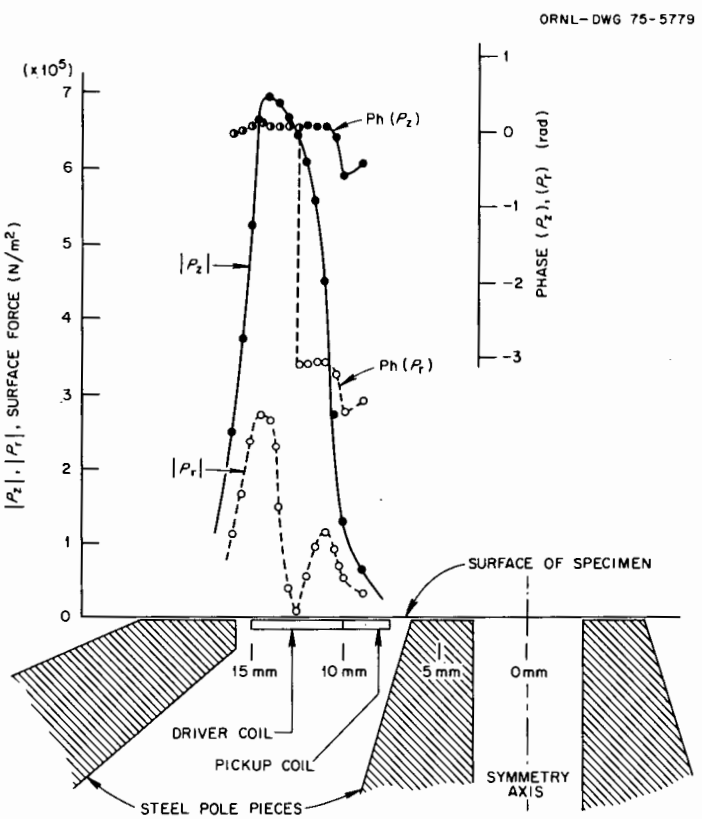

Fig. A5. Surface Forces Obtained Through Integration of Volume Forces of Fig. A4.

Figure A6 shows the approximations for the surface forces that are used for calculation of the ultrasonic field. From the vertical surface force, P_z, a relatively large amount of longitudinal wave and also a small amount of radially polarized transverse wave are generated because of the restraining characteristics of the solid surface.[4–7] From the horizontal and radial surface force, P_r, a relatively large amount of radially polarized transverse wave and also a small amount of longitudinal wave are generated because of the same characteristics of a solid surface.[4,5] Consequently, a displacement of a particle at an arbitrary point in a solid has four components: S_{zz}, a vertical component from the vertical surface force P_z; S_{rz}, a horizontal and radial component from the vertical surface force P_z; S_{zr}, a vertical component from the horizontal and radial surface force, P_r; and S_{rr}, a horizontal and radial component from the horizontal and radial force, P_r.

---

[4]Katsuhiro Kawashima, *The Theory and Numerical Calculation of the Acoustic Field Exerted by Eddy-Current Forces*, ORNL-5065 (in preparation).

[5]Katsuhiro Kawashima, *An Electromagnetic Transducer for Generation and Detection of Both Longitudinal and Transverse Ultrasonic Waves*, ORNL-5064 (in preparation).

[6]R. L. Roderick and R. Truell, "The Measurement of Ultrasonic Attenuation in Solids by the Pulse Technique and Some Results in Steel," *J. Appl. Phys.* 23(2): 267–79 (February 1952).

[7]F. Miller and H. Pursey, "The Field and Radiation Impedance of Mechanical Radiators on the Free Surface of a Semi-Infinite Isotropic Solid," *Proc. R. Soc. London Ser. A.*, 223: 521–41 (1954).

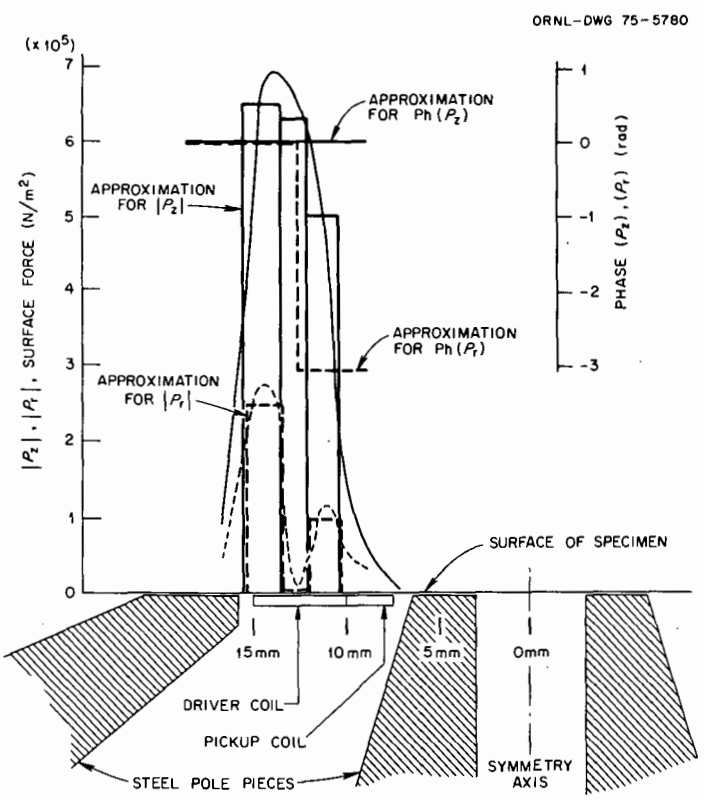

Fig. A6. Approximation of Surface Forces for Ultrasonic Wave Calculation.

The displacements S_z (= S_{zz} + S_{zr}) and S_r (= S_{rz} + S_{rr}) that are produced in sample 1 (stainless steel) by the electromagnetic transducer were calculated by use of the approximations of surface forces shown in Fig. A6. Figure A7 shows the displacements calculated for a distance of 58.3 mm from a point on the surface centered under the transducer. This distance corresponds to the location of the flaw near the symmetry axis in sample 1. Elastic constants that are necessary for the calculation were obtained from the wave velocities (C_ℓ = 5630 m/sec, C_t = 2690 m/sec), which were measured with the electromagnetic transducer, and density (7.85 g/cm^3, which was obtained by measuring the weight and volume of sample 1).

Figure A7 alone cannot explain all the characteristics of the electromagnetic transducer because of several reasons:

1. the efficiency of the pickup coil for ultrasound has not been considered;
2. the mode conversion efficiency between the longitudinal wave and the radially polarized transverse wave occurring at each reflection has not been considered quantitatively; and
3. several assumptions and approximations were made for the calculation.

However, Fig. A7 give us a fairly good field pattern of the electromagnetic transducer. The sharpness of the first peak of S_z (0–6°) may explain the sharp decrease of the F1 echo with displacement of the transducer in Fig. 15. The maximum particle displacement of about 30Å indicates that nonlinear elastic wave theory is necessary for an accurate description of the elastic wave fields produced by the electomagnetic transducer.

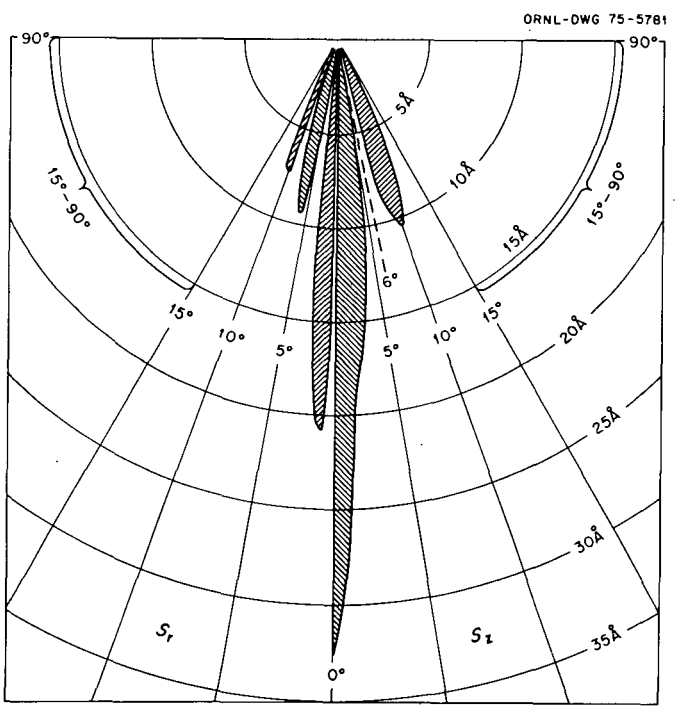

Fig. A7. Polar Distribution (distance is 58.3 mm) of Particle Displacements, S_z and S_r, Produced in Sample 1 by the Electromagnetic Transducer.

U'

ORNL-5063
UC-25 — Materials

INTERNAL DISTRIBUTION

(3) Central Research Library
ORNL — Y-12 Technical Library
Document Reference Section
Laboratory Records, ORNL RC
ORNL Patent Office
G. M. Adamson, Jr.
C. R. Brinkman
D. A. Canonico
K. V. Cook
F. L. Culler
J. E. Cunningham
J. H. DeVan
C. V. Dodd
G. G. Fee
B. E. Foster
W. O. Harms
R. F. Hibbs
(3) M. R. Hill
(20) K. Kawashima
A. L. Lotts
W. R. Martin
W. McClain
(20) R. W. McClung
H. E. McCoy
J. R. McGuffey
C. J. McHargue
P. Patriarca
S. Peterson
H. Postma
M. W. Rosenthal
J. L. Scott
W. A. Simpson, Jr.
G. M. Slaughter
J. H. Smith
S. D. Snyder
D. B. Trauger
T. N. Washburn
J. R. Weir, Jr.
G. D. Whitman
Advisory Committee:
John Moteff (consultant)
Hayne Palmour III (consultant)
J. W. Prados (consultant)
N. E. Promisel (consultant)
G. V. Smith (consultant)
D. F. Stein (consultant)

EXTERNAL DISTRIBUTION

ARGONNE NATIONAL LABORATORY, 9700 South Cass Avenue, Argonne, IL 60439

K. J. Reimann

GENERAL ELECTRIC COMPANY, 175 Curtner Avenue, San Jose, CA 95125

R. A. Day

HANFORD ENGINEERING DEVELOPMENT LABORATORY, P.O. Box 1970, Richland, WA 99352

J. C. Spanner

SANDIA CORPORATION, P.O. Box 5800, Albuquerque, NM 87115

D. W. Ballard

UNIVERSITY OF TENNESSEE, Department of Physics and Astronomy, Knoxville, TN 37916

L. Adler
W. E. Deeds

USERDA, DIVISION OF CONTROLLED THERMONUCLEAR RESEARCH, Washington, DC 20545

K. M. Zwilsky

USERDA, DIVISION OF REACTOR RESEARCH AND DEVELOPMENT, Washington, DC 20545

C. W. Cunningham
R. Hahn
E. E. Hoffman
K. E. Horton

USERDA, OAK RIDGE OPERATIONS, P.O. Box E, Oak Ridge, TN 37830

Director, Reactor Division
Research and Technical Support Division

USERDA, TECHNICAL INFORMATION CENTER, Office of Information Services, P.O. Box 62, Oak Ridge, TN 37830

(213) For distribution as shown in TID-4500 Distribution Category, UC-25 Materials.

☆ U.S. GOVERNMENT PRINTING OFFICE: 1975-748-189/46